Joule heating associated with auroral electrojets during magnetospheric substorms

X.-Y. Zhou,[1] W. Sun,[2] A. J. Ridley,[3] and S. B. Mende[4]

Received 11 June 2010; revised 1 November 2010; accepted 8 December 2010; published 3 March 2011.

[1] The magnetospheric substorm is important not only because it involves many interesting physical processes but also because it plays a key role in the solar wind energy dissipation into the ionosphere. This paper focuses on a quantitative description of the Joule heating production rate generated during substorms by auroral electrojets that are composed of two aspects: convection electrojets and the substorm electrojet. First, the natural orthogonal component (NOC) method is carefully discussed by examining its methodology and by comparing with other mathematical techniques and ionospheric observations. It is concluded that the NOC method is a very helpful and unique method that sheds insight into the electric potential patterns in the high-latitude ionosphere. Then, using the AMIE electric potential and the NOC method, the sawtooth event on 18 April 2002 and an isolated substorm on 15 November 2001 are studied. Electric fields and Joule heating rates corresponding to the convection electrojets and the substorm electrojet, respectively, are obtained. It is found that the Joule heating associated with the substorm electrojet is only one fourth to one third of that associated with the convection electrojets during the sawtooth event. However, the former dominated the total Joule heating during the expansion phase of the isolated substorm, and the two types of the Joule heating are comparable in magnitude in the isolated substorm recovery phase.

Citation: Zhou, X.-Y., W. Sun, A. J. Ridley, and S. B. Mende (2011), Joule heating associated with auroral electrojets during magnetospheric substorms, *J. Geophys. Res.*, *116*, A00I28, doi:10.1029/2010JA015804.

1. Introduction

[2] In the study of magnetospheric dynamics, substorms have drawn the highest attention not only because they involve many interesting physical processes (some of them are still not fully understood), but it also plays a key role in the solar wind energy dissipation in the ionosphere [e.g., *Perreault and Akasofu*, 1978; *Akasofu*, 1981; *Baker et al.*, 1985; *Kamide and Baumjohann*, 1985; *Rostoker et al.*, 1988]. This paper focuses on a quantitative illustration of the Joule heating production rate associated with auroral electrojets during substorms.

[3] Energy input to the ionosphere starts with the mechanical energy in the solar wind generator that gets converted to electromagnetic energy. That, in turn, is conveyed down the geomagnetic field lines (as Poynting flux) into the ionosphere, where it is dissipated through Joule heating. Joule heating in the ionosphere is given as $\mathbf{J} \cdot \mathbf{E}$ in the ionospheric rest frame, where $\mathbf{J}$ and $\mathbf{E}$ are the current and electric fields perpendicular to the magnetic field, $\mathbf{B}$. Thus, for an applied electric field, energy is dissipated by the current parallel to $\mathbf{E}$ (i.e., the Pedersen current); Hall current (perpendicular to $\mathbf{E}$) is nondissipative. That leads to a Joule-heating dependence on particle characteristic energy, because higher-energy particles penetrate more deeply into the ionosphere, where the Hall conductivity is greater than the Pedersen conductivity, and the currents tend to be nondissipative. Joule heating is then less important. Less energetic particles produce ionization at higher altitudes where Pedersen conductivities are greater than Hall conductivities and Joule heating is relatively more important [*Galand and Richmond*, 2001; *Vasyliũnas and Song*, 2005]. Since the Pedersen current density, J_p, is related to the Pedersen conductivity Σ_p and is expressed as $J_p = (\Sigma_p)E$, height-integrated Joule heating is given by

$$U_J = \mathbf{J} \cdot \mathbf{E} = J_p E = \Sigma_p E^2. \quad (1)$$

So far one of the most popular parameters used for the solar wind energy input into the magnetosphere is the ε function introduced by *Perreault and Akasofu* [1978] and *Akasofu* [1981] based on the Poynting flux ($\sim \mathbf{E} \times \mathbf{B}$). This energy coupling function is given as $\varepsilon = 10^7 V B^2 l_o^2 \sin^4(\theta/2)$, where $l_o = 7\ R_E$ denotes the effective magnetosphere radius, θ is the clock angle of the IMF from the north, V is the solar wind speed, B is the IMF strength and all parameters are in SI units. So ε presents the solar wind energy input rate in

[1]Jet Propulsion Laboratory, California Institute of Technology, Pasadena, California, USA.
[2]Geophysical Institute, University of Alaska Fairbanks, Fairbanks, Alaska, USA.
[3]Department of Atmospheric, Oceanic, and Space Sciences, University of Michigan, Ann Arbor, Michigan, USA.
[4]Space Sciences Laboratory, University of California, Berkeley, California, USA.

0148-0227/11/2010JA015804

Joule/s. The input solar wind energy is consumed by several processes in the magnetosphere, ionosphere and their connections. Three of the most important processes are: U_A, the rate of energy dissipation associated with the collision of precipitating auroral particles in the ionosphere; U_R, the rate of energy injection into the ring currents that flow in the magnetospheric equatorial plane; and U_J, the rate of the energy dissipation associated with the Joule heating in the ionosphere. So the total solar wind energy dissipation is estimated by $U = U_A + U_R + U_J$. U_A can be estimated using auroral brightness [*Rees et al.*, 1988; *Lummerzheim et al.*, 1997; *Germany et al.*, 1997; *Newell et al.*, 2001; *Vorobjev and Yagodkina*, 2008]; U_R using *Dst* [*Lu et al.*, 1998; *Turner et al.*, 2001] and U_J from *AE* [e.g., *Ahn et al.*, 1983], *PC* (the polar cap index) [*Chun et al.*, 1999], or *IL* (a local *AL* index resulted from the IMAGE magnetometer chain) [*Tanskanen et al.*, 2002]. But *AE* has limitations and cannot present substorm electrojets very well quantitatively during intensive storms or quiescent times when the auroral oval moves to the latitudes lower or higher than the AE stations that are located at 60.44°–71.21° magnetic latitude (MLAT) (http://wdc.kugi.kyoto-u.ac.jp/aedir/ae2/AEObs.html). Caveats of using *AE* index have been discussed by *Baumjohann* [1986].

[4] A better way to calculate U_J is to use equation (1). Since there are no direct measurements of the ionospheric conductivity and electric field, *Kamide and Baumjohann* [1985] developed an algorithm to obtained the parameters. They assumed that the height-integrated ionospheric conductivity is composed by two components. One is the background conductivity of solar UV origin [*Kamide and Matsushita*, 1979] and the other simulates substorm activity in the *AE* index [*Spiro et al.*, 1982]. They also assumed that the ionospheric electric field is derivable from an electrostatic potential, and a 2nd-order partial differential equation for the potential in terms of the associated equivalent current function has to be solved [*Kamide et al.*, 1981]. Using this method, *Kamide and Baumjohann* [1985] for the first time provided a Joule heating distribution in the ionosphere above 50° MLAT during an isolated substorm on 22 March 1979. They found that although the substorm auroral electrojets flow rather closely throughout the night sector, there are separate source regions of Joule heating. One is from the convection related DP2 current system and another is the substorm expansion related DP1 current. The source regions were not only in the evening and postmidnight sectors, but on the dayside. The cusp region was seen as one major heating source during substorms.

[5] In addition to the limitations of *Kamide and Baumjohann*'s [1985] method (e.g., the electric field is assumed to be electrostatic), there are controversies on the equivalent current that is conceptual and cannot be tested by real observations. Overall, their method provides a total Joule heating that actually has two components associated with convection electrojets and the substorm electrojet. In this paper, we avoid using the equivalent current. Instead, we use the assimilative mapping of ionospheric electrodynamics (AMIE) [*Richmond and Kamide*, 1988; *Ridley and Kihn*, 2004] electric potential. To obtain electric fields corresponding to convection electrojets and the substorm electrojet separately, the natural orthogonal component (NOC) method [*Faynberg*, 1975; *Sun et al.*, 1998, 2008] is employed, through which we are able to obtain the Joule heating rate associated with the convection electrojets (that is related to the magnetospheric and ionospheric convection) and with the substorm westward electrojet (that is related to the substorm current wedge). Consequently, our results provide an insight into the electric potential pattern in the high-latitude ionosphere and the Joule heating that is actually composed of the two elements during geomagnetic disturbances.

2. The Natural Orthogonal Component Method

[6] It is important and necessary to allocate a section discussing the NOC method, but the focus is on methodology. For the detailed mathematic description, interested readers can refer to *Sun et al.* [1998, 2008].

2.1. The NOC Method as a Physical Insight

[7] While formulas in the NOC method are not physical equations, the method has a clear and strong physical indication. By solving an eigen equation, the solution of Schrödinger equation in the quantum mechanics provides allowable energy states of the quantum. Similar to the Schrödinger equation, the NOC method solves an eigen equation [*Sun et al.*, 1998; *Baker et al.*, 2003]. Consequently, the solution provides a natural basis that corresponds to a set of eigenfunctions each of which indicates an allowable electric potential state.

[8] This unique signature allows the NOC algorithm to separate the electric potential in the polar cap into many possible potential configurations. The priority of each configuration is given by its corresponding eigenvalue that varies in a range of several orders. The most important and significant point is that in the NOC results it has always been the case that a two-cell pattern and/or a one-cell pattern are the most allowable potential patterns shown by the first and second eigenvalues that are about an order of magnitude higher than other possible potential patterns. Figure 1 (top) shows the eigenvalue, λ_k, as a function of its order number K. Contributions of possible potential patterns decrease with increasing K order. Note that the 15 July 1997 event is a steady magnetospheric convection (SMC) event and the 18 April 2002 is a sawtooth event. Both events are driven by a magnetic cloud. NOC separation results have shown that the most possible and allowable potential pattern that is indicated by λ_1 (and λ_2 for the SMC event) is a two-cell convection pattern. Figure 1 (bottom) quantitatively depicts the contribution of the first K patterns to the total potential. In general, patterns with corresponding first two eigenvalues contribute ~75% or more of the total electric potential. Thus, the first two potential patterns dominate the polar cap potential. Higher orders of $K > 8$ contribute ~10% of the total potential, which are related to less possible and fairly random processes.

[9] By separating the total potential into different patterns, corresponding electric fields can be calculated by differentiating the potential. The two-cell potential pattern dominates the polar cap potential pattern, though sometimes it becomes more complicated when substorm expansion phases (SEPs) take place. The responsible potential pattern for SEPs is expected to be one cell near the midnight auroral zone because it provides a southward electric field that drives a substorm westward electrojet as the ionospheric

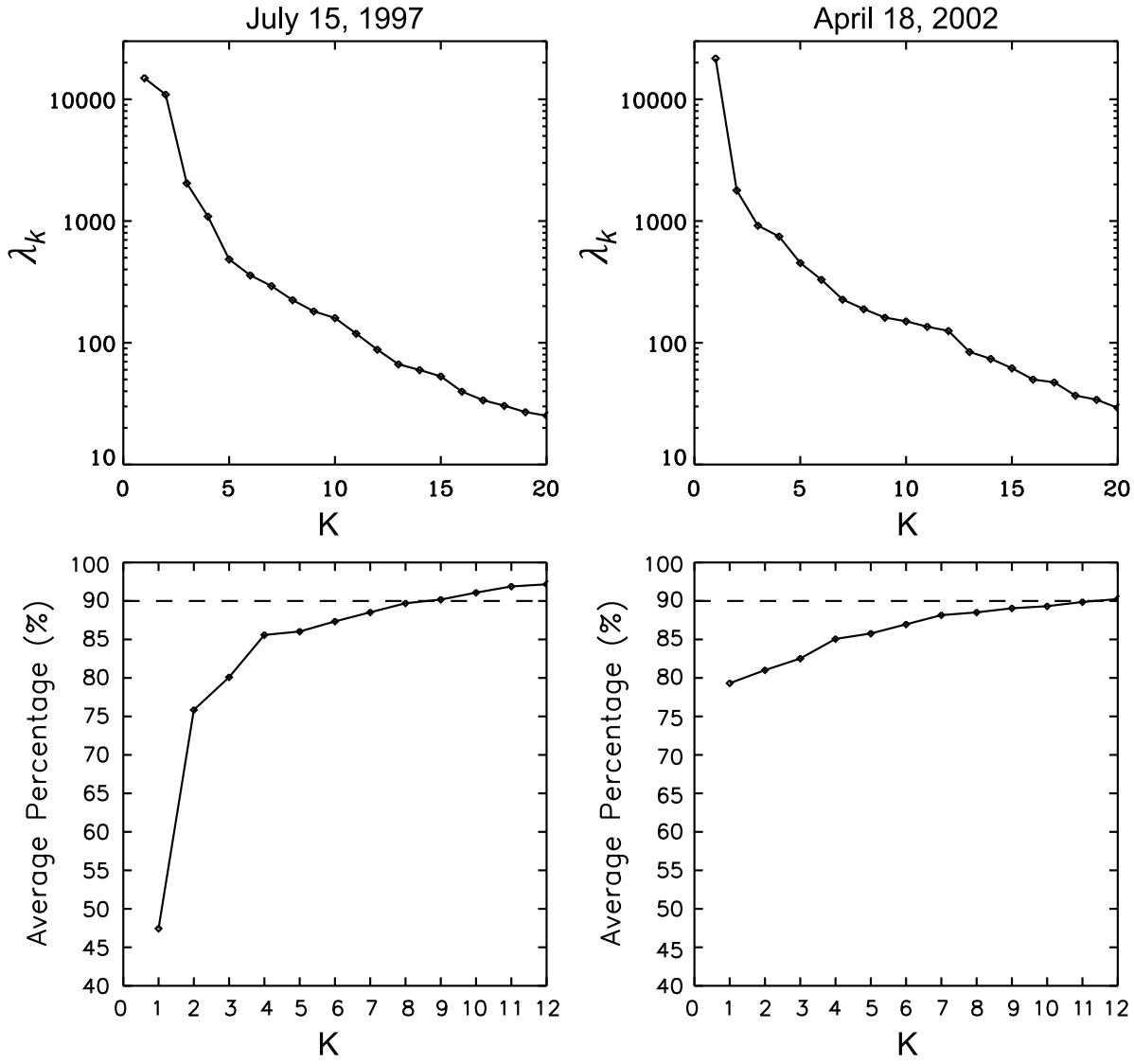

Figure 1. Eigenvalue variation and corresponding significance: (top) eigenvalues (λ_k) in order [*Sun et al.*, 2008; *Zhou et al.*, 2008] and (bottom) the ratio of the potential of the first K eigenfunctions to the total potential. For example, when $K = 8$ for the 15 July 1997 event, the average percentage of 90% means that an integrated contribution of the first eight eigenfunctions contribute 90% of the total potential. The average percentage is a daily average. For the 15 July 1997 event (which is also called a steady magnetospheric convection (SMC)), both the first and second eigenvalues, λ_1 and λ_2, appear to be very large. The corresponding potential patterns are two-cell patterns, which contribute ~75% of the total potential. For the 18 April 2002 sawtooth event, λ_1 presents a two-cell convection pattern, and λ_2 presents a one-cell substorm expansion pattern. Contribution of the first eigenfunction is ~80% of the total potential, indicating strong convection, which is consistent with the long and intense southward IMF condition during a magnetic cloud.

closure of the substorm current wedge. This scenario is described by *Kamide et al.* [1994] and shown in Figure 2a. A one-cell potential is developed during SEP at lower latitudes near midnight. Meanwhile the enhanced plasma convection will intensify the preexisting two-cell potential. Often observed patterns are complex during substorms, which might have been due to the combination effect of the high-potential areas (shaded in gray). Actually, such a scenario is well supported by the statistical analysis of *Cai et al.* [2006] in which one-cell substorm potential patterns were obtained via subtracting a background electric potential pattern [*Weimer*, 1996] from the AMIE potential.

[10] Using the NOC method and AMIE potential data, we were able to separate the polar cap potential into a two-cell pattern (Figure 2b) occupying the cap and a one-cell pattern (Figure 2c) centered in midnight sector below 70° MLAT [*Sun et al.*, 2008; *Zhou et al.*, 2008]. This consistency with *Kamide et al.*'s [1994] prediction in Figure 2a, with the DP1 and DP2 concept [*Clauer and Kamide*, 1985], and with previous studies of *Weimer* [1996] and *Cai et al.* [2006] is not a coincidence; instead, is an indication of the signifi-

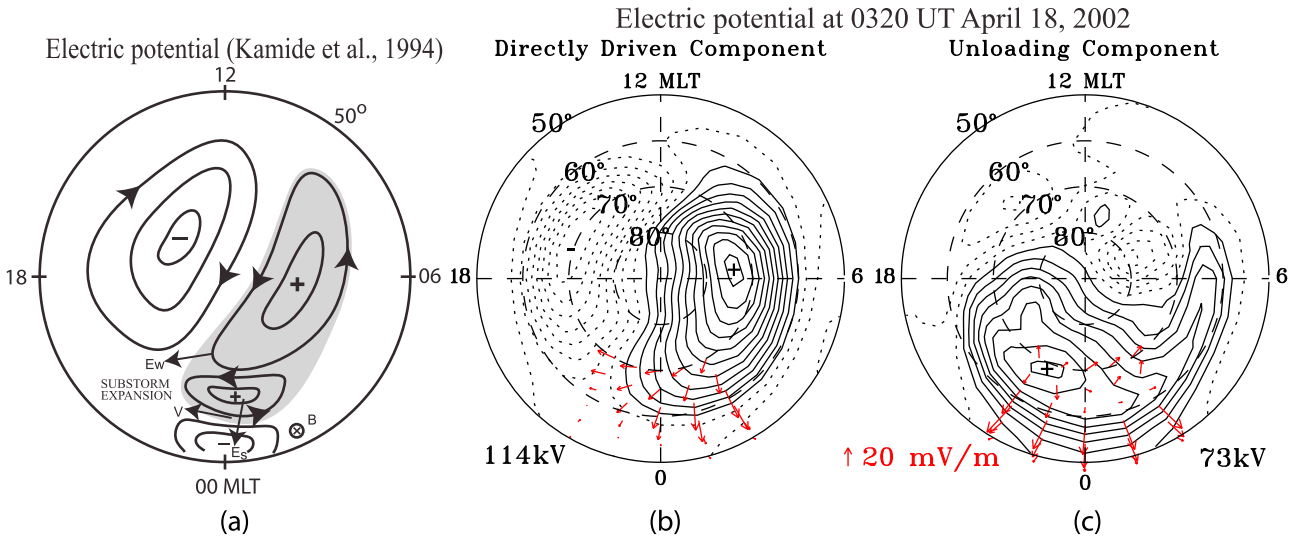

Figure 2. Polar cap potential patterns and their physics. (a) A schematic diagram of separating a complicated substorm time polar cap potential configuration into a two-cell convection pattern around the magnetic pole and a one-cell pattern at lower latitudes near midnight. The two-cell potential is enhanced because of increasing plasma convection. The one-cell potential is the ionospheric manifestation of the substorm current wedge in the magnetosphere. The shaded high-potential areas combine the two effects, which creates the complexity of the polar cap potential configuration during substorms. Although the one-cell pattern is not common in the potential observations, the two-cell convection pattern has been widely reported by SuperDARN observations and MHD simulations. The westward electrojet flowing in the **V** direction is driven by $-\mathbf{E_s} \times \mathbf{B}$ [*Kamide et al.*, 1994]. (b) The two-cell electric potential pattern separated using the NOC method at 0320 UT 18 April 2002 during a sawtooth event [*Sun et al.*, 2008]. Its corresponding eigenvalue is shown in Figure 1 at $\lambda_1 = \sim$11,000, indicating an intense ionospheric convection driven by a magnetic cloud. (c) The one-cell electric potential pattern separated using the NOC method at 0320 UT for the same day as in Figure 2b [*Sun et al.*, 2008]. The corresponding eigenvalue is about an order lower than the first. Arrows in the midnight sector (2200–0200 LT, 50°–70° MLAT) are corresponding electric fields.

cance of the NOC method. Solutions of the NOC eigen equation provide a natural base of possibly allowed potential patterns in the polar cap, which are of fundamental importance for magnetospheric physics. Furthermore, corresponding electric fields in the midnight sector (2200–0200 LT) have been calculated (shown as red arrows in Figures 2b and 2c) and found to be a westward dominant electric field in the two-cell pattern and a southward electric field in the one-cell pattern. One way to explain the establishment of the southward electric field is that the westward electric field drives a westward Pedersen current and an enhanced northward Hall current when the local conductivity is higher than in the surrounding region because of precipitating auroral electrons. A southward polarization electric field would be gradually generated by the accumulated charges due to the northward Hall current if the current cannot be completely closed via field-aligned currents [*Baumjohann et al.*, 1981; *Kan*, 2007]. This southward electric field drives a secondary westward Hall current that combines with the westward and primary Pedersen current, thus to form the so-called westward Cowling current [*Boström*, 1964; *Coroniti and Kennel*, 1972].

2.2. Comparison With Observations

[11] To further confirm the NOC method's significance, in this section we compare the NOC results with observations in the magnetosphere and ionosphere. Figure 3 shows the comparison with geomagnetic dipolarizations measured at the geosynchronous orbit. The event is well documented sawtooth event on 18 April 2002 [e.g., *Lui et al.*, 2004; *Henderson et al.*, 2006; *Ohtani et al.*, 2007]. In Figure 3a (from top to bottom) are the *AL* and *AE* indices, the unloading (UL) electric field in the ionosphere (i.e., the southward electric field corresponding to the SEP evolution) obtained from the NOC method, and the geomagnetic field B_z component measured by GOES 10. The three shaded areas are centered at the magnetic field dipolarization that has been widely accepted as one of important evidences of SEP onsets in the magnetosphere. There is a clear anticorrelation between *AL* and *AE* even to the naked eye, especially during the shaded durations. Variations between the UL component in the ionosphere and the B_z component in the magnetosphere are very well consistent to the eye. However, at every dipolarization, *AE* (*AL*) decreased (increased), which is an abnormal *AE* (*AL*) behavior during a substorm expansion phase. The worst case was the last duration around 0800 UT during which *AE* and the B_z dipolarization are anticorrelated with a high correlation coefficient at 0.82. This result suggests that caveat should be considered when using *AE* (or *AL*) as an indicator of substorm expansions during storms.

[12] To quantitatively describe the relationship, correlation coefficients are calculated and shown in Figure 3b.

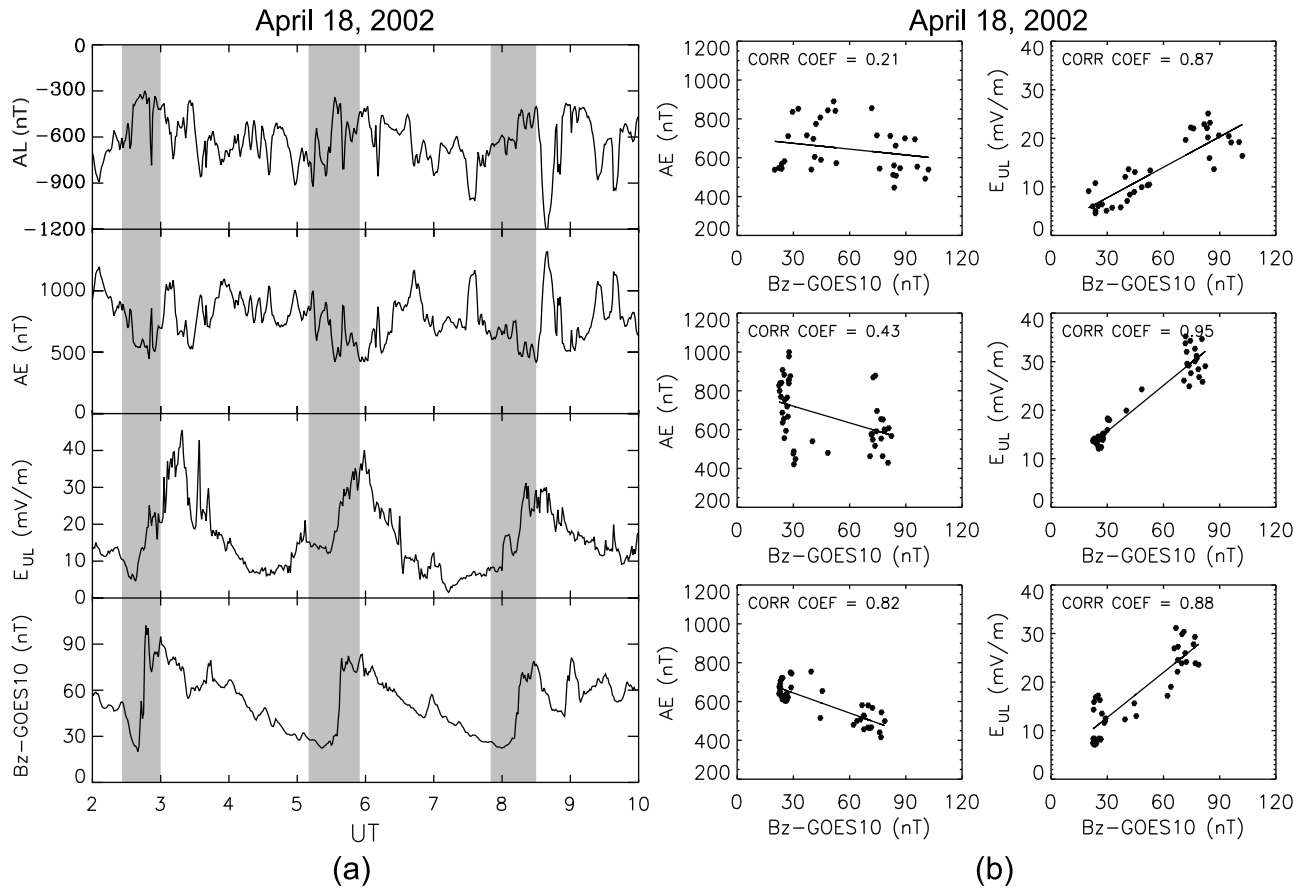

Figure 3. (a) Correlation between NOC-identified SEP onsets and the magnetic dipolarizations at the geosynchronous orbit. E_{UL} are maxima in the midnight section (2100:03 MLT and 50°–70° MLAT) [*Sun et al.*, 2008]. (b) Correlation coefficients in the shaded areas of Figure 3a.

Figure 3b (left) shows the correlations between *AE* and the B_z component at GOES 10 corresponding to the three SEP onsets from top to bottom. As shown by the linear fittings, *AE* is anticorrelated with the B_z variation (the same anticorrelation exists between the *AL* magnitude and B_z at GOES 10, but it is not shown here). Therefore, the higher the correlation coefficient, the more misleading is the *AE* index. The conclusion is that *AE* (as well *AL*) cannot be used as a SEP proxy for this sawtooth event. In contrast, Figure 3b (right) shows the correlation coefficients between the UL component and B_z at GOES 10, which are all positive with values of 0.87 or more. This high correlation confirms that SEP onsets identified using the NOC method are reasonably accurate and reliable.

[13] Another comparison is between the electric fields obtained using the NOC method and those observed from balloon flights in the northern hemisphere nightside auroral zone. Figure 4a is the averaged ionospheric electric fields of 19 substorms obtained from balloon measurements near midnight between $L = 6.6$ and 8.3. The 5 h electric fields are centered at SEP onsets, i.e., the 0 h [*Mozer*, 1971]. From top to bottom, panels in Figure 4a are the westward, southward and total electric field (i.e., the square root of the sum of the squares of the top two curves). The vertical line at 0 h marks the time when the SEP onset started. Mozer's observations show that the westward electric field increased from ~0 to 20 mV/m during the substorm growth phase and was relative stable during the SEP. The southward electric field was low and near zero during the substorm growth phase but suddenly increased to ~30 mV/m at the SEP onset. Mozer's balloon-based measurements confirmed that there is a suddenly enhanced southward electric field when the substorm westward electrojet develops. Later *Carlson and Kelley* [1977] and *Baumjohann et al.* [1981] observed the same signature.

[14] Taking a superposed epoch average of the three substorm events shown in Figure 3, the westward (E_{DD}), southward (E_{UL}) and total electric fields are shown in Figure 4b with the same format of Figure 4a. E_{DD} and E_{UL} were obtained using the NOC method from the two-cell and one-cell patterns (i.e., the max electric field in the selected sector at a given time as shown in Figure 2). Since the quasiperiodicity of the sawtooth event is ~2–3 h, we only use 1 h before and 1 h after the SEP onset to reduce the effect of nearby substorms. Note that the sawtooth occurred in a storm that was driven by a magnetic cloud. So the averaged E_{DD} appeared to be relative stable. The E_{UL} (E_{TOT}) abruptly increased from ~5 to 30 mV/m (from ~10–40 mV/m) at the SEP, which is consistent with *Mozer*'s [1971] observations. Figure 4c shows the NOC result of an isolated substorm event. More detailed information about the substorm will be discussed in section 3. Identified

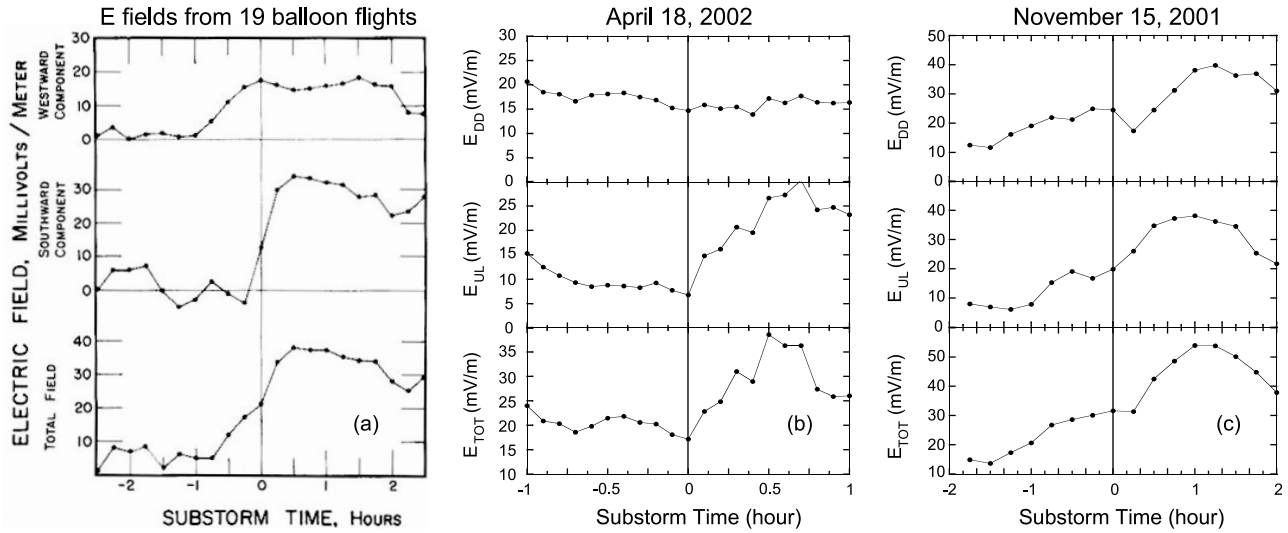

Figure 4. Comparisons between NOC-identified ionospheric electric fields and observed electric fields from 19 balloon flights. (a) The 15 min averages of the E-W and N-S components of the *E* field obtained during 19 balloon flights. The total electric field at the bottom is the square root of the sum of the squares of the top two components [*Mozer*, 1971]. The 5 h electric fields are centered at SEP onsets, i.e., the 0 h where there is a vertical line marking the time of the SEP onsets. (b) Electric fields separated using the NOC methods for the three SEPs in Figure 3 averaged and shown in the same format as Figure 4a. E_{DD} means the direct driven component, i.e., the westward electric field; E_{UL} is the unloading component, i.e., the southward electric field. More details of the NOC analysis of the 18 April 2002 event can be found in the work by *Sun et al.* [2008]. (c) Separated E_{DD} and E_{UL} using the NOC method for an isolated substorm on 15 November 2001 with minimum *AL* at ~1000 nT (more information can be seen in Figures 6 and 7).

electric fields are shown here first to compare to Mozer's observations. During this isolated substorm, E_{DD} not only increased during the substorm growth phase, but also in the expansion phase and almost by a factor of 2 from ~20 mV/m at the SEP onset to ~40 mV/m at the SEP peak. Meanwhile, E_{UL} abruptly increased ~20 mV/m within 30 min after the onset, which is consistent with Mozer's observations and the E_{UL} variation in Figure 4b. It has been widely acknowledged [e.g., *Kan*, 2007] that current sheet disruption, magnetic reconnection are possible generation mechanisms of SEP onset. These processes should also enhance the magnetospheric and ionospheric convection, which explains the E_{DD} enhancement as seen in Figure 4c (top).

[15] The above comparisons with the geomagnetic and electric field observations confirmed the significance of the NOC method and its potential support in understanding the ionospheric potential patterns in the polar cap, which is of fundamental importance to the magnetospheric dynamics.

3. Joule Heating in the High-Latitude Ionosphere During Substorms

[16] This study uses the AMIE electric potential and the NOC method. The AMIE potential that is determined from the assimilation of magnetometer data worldwide provides the electric potential above 44° MLAT. Four steps are taken in this study to obtain the Joule heating. First, obtain the AMIE potential data from its homepage at the University of Michigan (http://amie.engin.umich.edu/). The data have a 2° resolution in latitude and 15° in longitude and a time resolution of 1 min. So the grids number in total is 576. Second, separate the AMIE potential into different patterns using the NOC method. Differentiate the potential in the two-cell pattern (as shown in Figure 2b), to obtain the directly driven electric field (the arrows in Figure 2b), E_{DD}. Likewise, differentiate the potential in the one-cell pattern (as shown in Figure 2c), to acquire the unloading electric field, E_{UL}. Third, calculate the ionospheric Pedersen conductivity in the high-latitude area above 50° MLAT using *Ahn et al.*'s [1983] model. Fourth, calculate the Joule heating using equation (1), i.e., $JH_{DD} = \Sigma_p E_{DD}^2$, $JH_{UL} = \Sigma_p E_{UL}^2$. To have a more comprehensive understanding of the Joule heating during substorms, we examined some storm time substorms (the April 2002 sawtooth event) and an isolated substorm.

3.1. The Joule Heating During Storm Time Substorms

[17] Since the April 2002 sawtooth event has been well documented, we do not describe the event in this paper. Interested readers can find the solar wind condition, magnetospheric activity and ionospheric auroral information from relevant articles [e.g., *Lui et al.*, 2004; *Henderson et al.*, 2006; *Ohtani et al.*, 2007]. The electric potential patterns and separated electric fields obtained using the NOC method can be found in work by *Sun et al.* [2008] and *Zhou et al.* [2008]. Figure 5 illustrates the electric fields, corresponding Joule heating (in red), and global integrated Joule heating, and the *AL* index. The electric field is taken as the maximum magnitude at every minute on the nightside (1800:06 magnetic local time (MLT)) and 50°–70° MLAT region composed of 120 grid points. Note there is one electric field vector for each grid that is 2° in latitude and 15° in longitude. Only the one with maximum value was taken into account. The direction of this vector was not considered. However, as shown in Figure 2, the direction of maximum

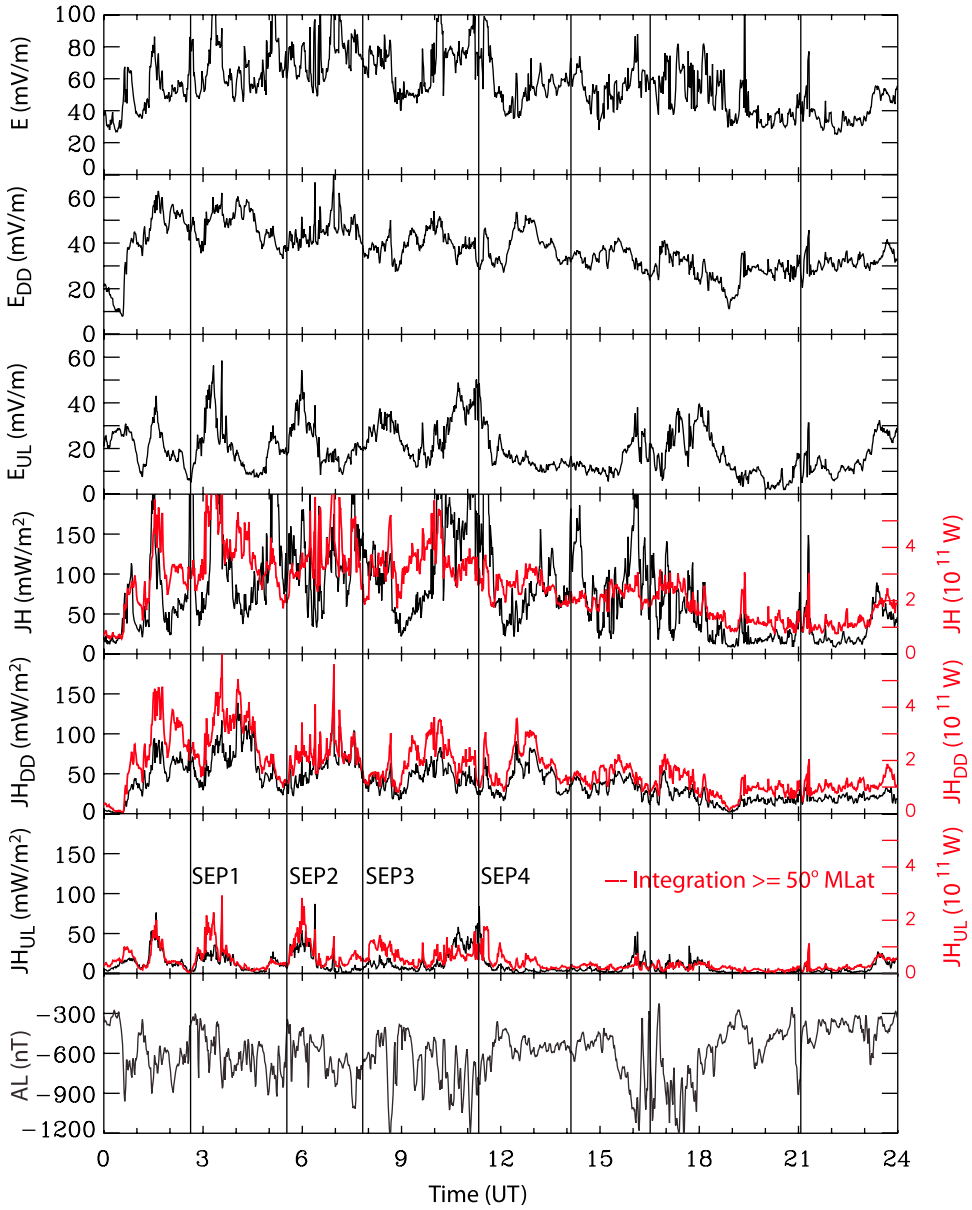

Figure 5. NOC results of electric fields and corresponding Joule heating of the 18 April 2002 sawtooth event. (top to bottom) The total electric field obtained from the AMIE potential; the directly driven (corresponding to the convection electrojets) electric field (E_{DD}) and the unloading (corresponding to the substorm electrojet) electric field (E_{UL}); the total Joule heating (JH) derived from the total electric field and the Pedersen conductivity; the Joule heating associated with convection electrojets (JH_{DD}) and the Joule heating associated with the substorm electrojet (JH_{UL}); and the *AL* index. The electric fields are maxima in the nightside region (1800:06 MLT, 50°–70° MLAT). Those who are also interested in the location of the maxima can refer to Figure 2 and *Sun et al.* [2008, Figure 4], in which electric field vectors are superposed on the electric potential 2-D distribution. Red curves in the fourth to sixth panels are global Joule heating integrated in all local time from and above 50° MLAT. Therefore, the comparison between Joule heating components can be reasonable. Two-dimensional Joule heating distributions (not shown here) indicate that the Joule heating is primarily along the auroral oval where the Pedersen conductivity is the most intense. The two integrated Joule heating components primarily present the Joule heating along convection electrojets and along the substorm electrojet.

E_{DD} is expected to be westward and E_{UL} to be southward in the auroral oval. Correspondingly, the Joule heating rates are the maximum values. To obtain a reasonable comparison, the Joule heating is integrated over the entire high-latitude region from 50° MLAT poleward, including all local times and is shown in red. The vertical lines are the times when energetic particle injections were observed by LANL satellites [*Henderson et al.*, 2006]. Marks of SEP1 to SEP4

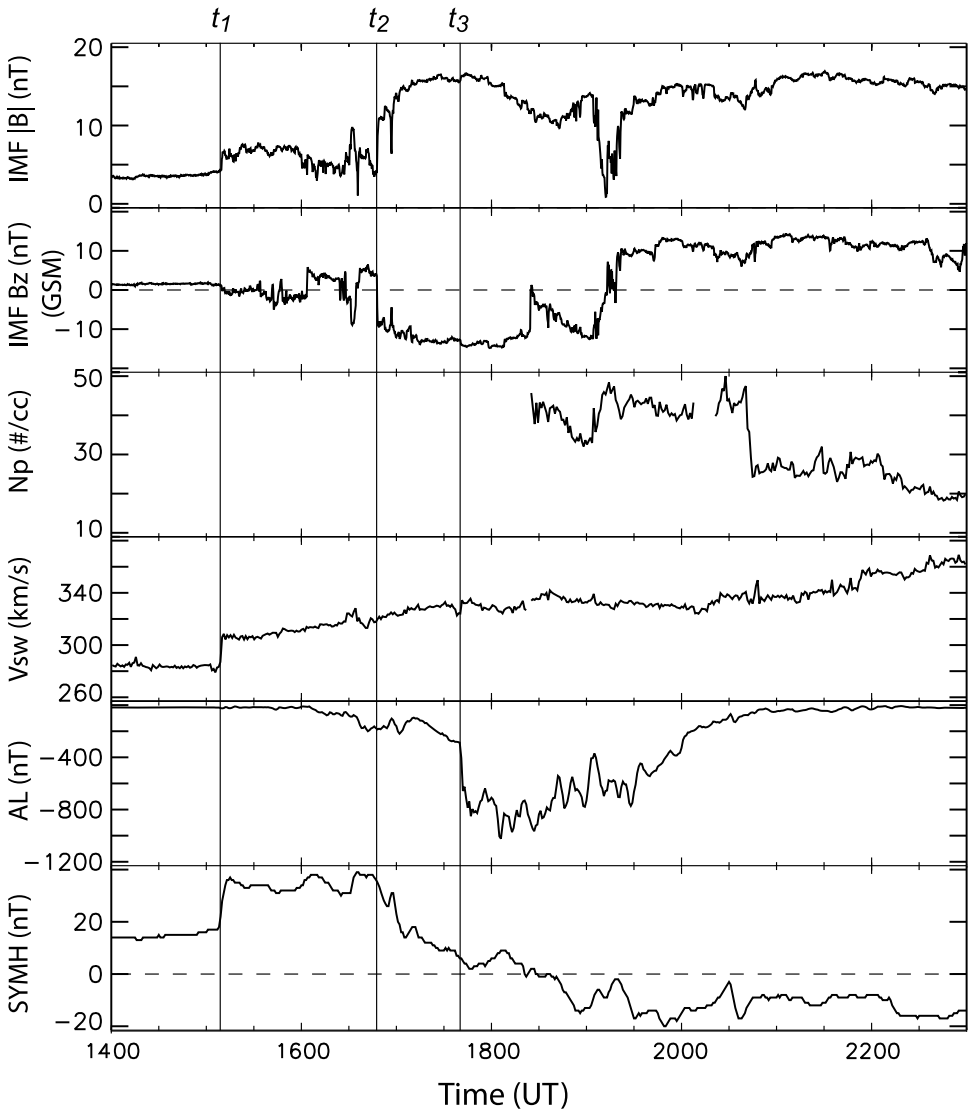

Figure 6. Solar wind parameters and geomagnetic indices for the isolated substorm on 15 November 2001. The solar wind data have been shifted 1 h and 15 min to the subsolar magnetopause.

in Figure 5 (sixth panel) are the SEPs indentified using the IMAGE/FUV auroral images [*Lui et al.*, 2004]. The 2-D distribution of Joule heating was basically determined by the Pedersen conductivity, though the local magnitude variation during SEP was primarily due to electric field variations.

[18] In the E_{DD} and E_{UL} panels, at each SEP the E_{UL} increased ~30 mV/m or more. *Sun et al.* [2008] commented that when E_{UL} increases and reaches to ~30–40 mV/m, SEP will take place. It is also evident that E_{DD} increased ~30% during the SEP, though the E_{DD} enhancements were not shown by the average in Figure 4b. The total Joule heating in Figure 5 (fourth panel) is at a level comparable to that shown on the AMIE Web site and to results of other events from *Baker et al.* [1985] and *Kamide and Baumjohann* [1985]. A very interesting result is that during this storm time substorm event, the convection related Joule heating, JH_{DD}, dominated the energy dissipation and reached its peak during SEP. Surprisingly, the Joule heating associated with the substorm electrojet is very minor at a level that can be ignored except in the ~1 h intervals centered at the peaks of E_{UL}. Even then the JH_{UL} is a factor of ~2 less than the JH_{DD}. This result indicates that the ionospheric Pedersen conductivity (especially the dayside) plays a key role in the Joule heating instead of the electric field. In addition, in the substorm electrojet region, the Pedersen conductivity is not as significant as that in the intense convection region.

3.2. The Joule Heating During an Isolated Substorm

[19] The solar wind and geomagnetic *AL* and *SYMH* indices for the isolated substorm on 15 November 2001 are shown in Figure 6. The ACE solar wind data have been shifted 1 h and 15 min to the dayside magnetopause assuming at 10 R_E. At time t_1 an interplanetary shock is detected (but there is a data gap in the proton density). It caused a sudden enhancement in *SYMH* to ~38 nT. Downstream of the shock, the solar wind ram pressure might have kept high and resulted in a high *SYMH* about an hour until t_2 when the IMF B_z suddenly turned to southward. The *SYMH* index started to reduce to near zero at t_3 when the SEP onset took place. In the SEP, AL reached about −1000 nT and the

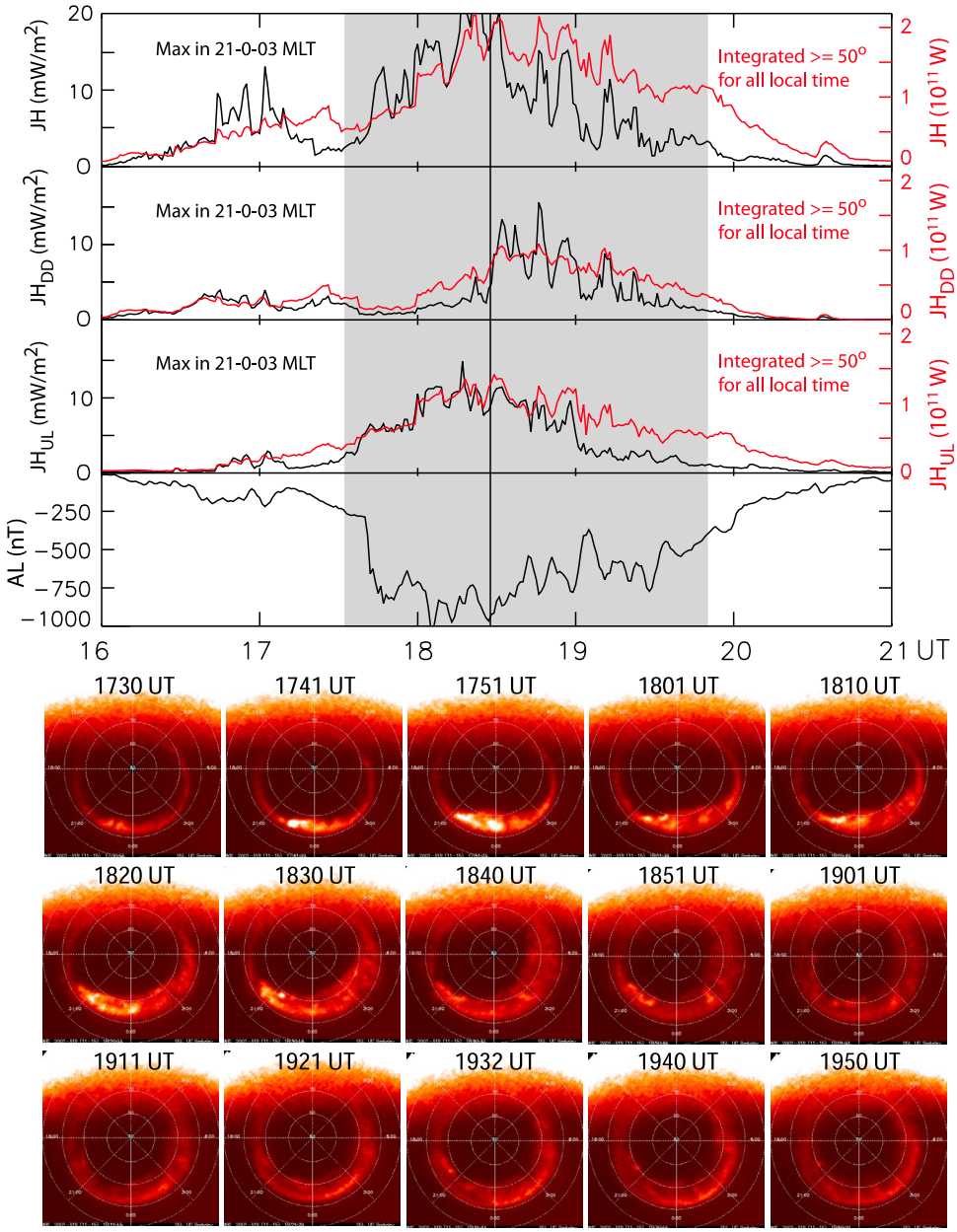

Figure 7. Joule heating and auroral activity of the 15 November 2001 substorm. Parameters in each panel are the same as those in the fourth to sixth panels of Figure 5. Auroral images, which are from the IMAGE/FUV, show the auroral westward, eastward, and poleward expansion during the SEP.

SEP lasted ~2 h. The magnitude of *SYMH* kept low and less than 20 nT, indicating there was no storm activity.

[20] Figure 7 shows the Joule heating in the midnight sector (2100:03 MLT and 50°–70° MLAT) and global integration (in red). The Joule heating in black is obtained from the maximum electric field as described in Figure 5. The substorm interval is shaded and corresponding auroral activity is shown below by the IMAGE/FUV images. The SEP onset was at ~1740 UT when the *AL* index suddenly turned further negative and the aurora broke up at ~2200 MLT. The aurora expanded polarward and reached the high latitude of ~72° MLAT near midnight at ~1825 UT indicated by a vertical line in Figure 7. Then, the substorm recovery phase started and the auroral brightness decayed. However, the auroral oval latitudinal width kept increasing and covered ~20° in latitude around 0500 MLT at 1840 UT. The total and separated electric fields are not shown in Figure 7 but can be found in Figure 4c. The E_{DD} increased from ~10 to 20 mV/m during the growth phase, which is consistent with the southward IMF B_z that started from t_2 in Figure 6. About 1 h after the SEP onset, the E_{DD} reached the maximum of 40 mV/m, and then the recovery phase began. The E_{DD} reduced to 20 mV/m at ~2000 UT near the end of the substorm. The E_{UL} increased ~10 mV/m in growth phase as well because of the same reason of the E_{DD} enhancement, but the major increase of ~20 mV/m occurred during the SEP. For this isolated substorm, JH_{UL} and JH_{DD} are of the same level. During the SEP (which is in ~1740–1825 UT)

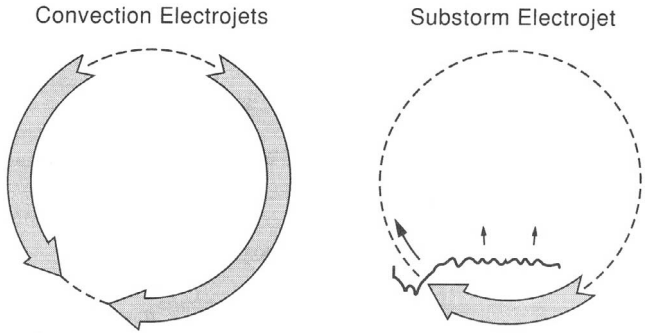

Figure 8. Sketch of auroral electrojets: convection and substorm electrojets (adapted from *Baumjohann and Treumann* [1997, Figure 5.13], copyright 1997, reproduced with permission from Imperial College Press). The DD and UL components discussed in this paper correspond to these two types of electrojets, respectively.

both the localized maxima and the globally integrated JH_{UL} dominated the total Joule heating. Contributions of JH_{DD} in the midnight (the black curve) were negligible. The JH_{DD} became comparable to the JH_{UL} in the recovery phase after ~1830 UT. More studies need to be done to understand whether this is a coincidence with the enhanced auroral oval width on the dawnside, which might be an indication of intensified plasma convection.

4. Discussion and Conclusion

4.1. Further Comments on the NOC Method

[21] Analogous to many mathematical methods, algorithms, and techniques employed in space physics (such as FFT, power spectrum analysis, wavelet analysis, filtering, minimum variance analysis etc.), the NOC method is composed of some algorithms. The NOC uniqueness is that it is on the basis of natural orthogonal component. Using mathematical tools is not a mistake or weakness of any of these methods. Whether a method is significant should be evaluated based on the returned result and the revealed physics. As a matter of fact, the space physics community has benefited from the minimum variance analysis, FFT, etc.

[22] The NOC method and its results present a wide and potential further application of the existing huge amount of observations from the ground-based magnetometers, radars and near Earth satellites. For example, by combining the NOC technique with the AMIE electric potential, the AMIE website will be able to provide separated potential patterns and corresponding electric fields and Joule heating production rates in addition to its current ionospheric property productions. Similar applications of the NOC method can be done with the SuperDARN and SuperMAG. As a result, the communities of magnetosphere and ionosphere will obtain not only direct measurement data, observation assimilations, but also further physical information in terms of the separated potential pattern, electric field and Joule heating. Actually, *Matsuo et al.* [2002] utilized a similar method, the empirical orthogonal function (EOF) analysis, to characterize dominant modes of two-dimensional high-latitude electric field variability based on one-dimensional plasma drift measured by DE 2 satellite. They found that 11 EOFs are capable of presenting ~68% of the squared electric field. Using the NOC method, *Baker et al.* [2003] analyzed the relationship between the auroral brightness and the interplanetary parameters; and found the temporal coefficients for the various eigenmodes are correlated separately with solar wind parameters and IMF components. The dominant influence of the southward IMF B_z component was confirmed. The solar wind density and IMF B_x and B_y only affect the subtle relationships.

[23] In addition to the NOC advantages and potential applications, a caveat should be mentioned. As many other analysis methods, the NOC output heavily depends on the accuracy of input data. In this study, the AMIE potential is utilized. The AMIE potential is obtained by assimilating the worldwide magnetometer data. It is not rare when there is a data gap in the polar cap (such as the lack of magnetometer stations in Russia). Some techniques can be used for "best fitting" to the data gap, but caveat should be considered for explaining the NOC output when such gap exists. By saying this, however, the function and capability of the NOC method still stand.

[24] We conclude that the NOC method is a very helpful method. Its application includes obtaining separated electric fields of E_{DD} and E_{UL} and the corresponding Joule heating rates, which have not been accomplished by any other methods. The results help us to understand the substorm importance in terms of the energy dissipation in the ionosphere in the form of Joule heating.

4.2. Convection Electrojets and Substorm Electrojet

[25] Auroral electrojets discussed in the paper include two aspects, convection electrojets (as illustrated in Figure 8, left) and the substorm electrojet (as illustrated in Figure 8, right). There have been studies and descriptions of these ionospheric current flows in the middle and high latitudes during storms and substorms [e.g., *Baumjohann and Treumann*, 1997; *Cravens*, 1997]. Two-cell convection pattern is formed when the ionospheric plasma flows across the polar cap from noon to midnight and returns to the dayside via paths on the dawn and dusk sides at lower latitudes. These return paths give rise to the convection electrojets. The convection electrojets are strengthened or weakened when the IMF B_z turns southward or to zero/northward, respectively. E_{DD}, examined in this paper, is the electric field that drives this plasma convection. In contrast to the convection electrojets, the substorm electrojet is the ionospheric closure of the substorm current wedge that is diverted from the cross tail current via field-aligned currents. Therefore, the substorm electrojet flows in the midnight sector and only evolves in SEP when the substorm current wedge is established. However, the development of the substorm electrojet is mainly determined by the enhanced ionospheric conductivity due to a massive particle precipitation at the SEP onset and during the SEP evolution that are visualized as an auroral breakup and abrupt poleward and westward surge. E_{UL}, examined in this paper, accompanies this substorm electrojet as we have discussed in section 2 and Figure 2.

[26] Taking the unique advantage of the NOC method, for the first time we have provided quantitative description of the Joule heating associated with the convection electrojets and the Joule heating with the substorm electrojet. The

results indicated that during the April 2002 sawtooth event JH_{UL} plays only a minor role in terms of the energy dissipation. On average, JH_{DD} is of ~2.5×10^{11} W (in the first half day from 0000 to 1200 UT) that is a factor of 3–4 higher than the JH_{UL} that has an average of ~0.75×10^{11} W during this interval. During the isolated substorm, JH_{UL} dominated the total Joule heating during the expansion phase. In the midnight sector, JH_{DD} was negligible, which indicates that the convection electrojets in this area play a minor role in the Joule heating. In the recovery phase, JH_{UL} and JH_{DD} became comparable in magnitude indicating an enhanced convection electrojets. This variation in JH_{DD} might be due to the time delay between the SEP onset in the tail and the enhanced convection in the auroral ionosphere. Interestingly, the JH_{UL} in the sawtooth event is about a factor of 2 higher than the JH_{UL} in the isolated substorm though the *AL* index of the two events was of the same level. This finding adds a caveat on using *AL* or *AE* as an estimate of the substorm Joule heating.

[27] **Acknowledgments.** The results reported here represent one aspect of research carried out by the Jet Propulsion Laboratory, California Institute of Technology, under a contract with the National Aeronautics and Space Administration. Research at the University of Michigan was supported by NSF grant ATM-0639336 and by AFOSR grant FA9550-070434.

[28] Robert Lysak thanks Gordon Rostoker and another reviewer for their assistance in evaluating this paper.

References

Ahn, B.-H., S.-I. Akasofu, and Y. Kamide (1983), The Joule heat production rate and the particle energy injection rate as a function of the geomagnetic indices *AE* and *AL*, *J. Geophys. Res.*, *88*, 6275–6287, doi:10.1029/JA088iA08p06275.

Akasofu, S.-I. (1981), Energy coupling between the solar wind and the magnetosphere, *Space Sci. Rev.*, *28*, 121–190, doi:10.1007/BF00218810.

Baker, D. N., T. A. Fritz, R. L. McPherron, D. H. Fairfield, Y. Kamide, and W. Baumjohann (1985), Magnetotail energy storage and release during the CDAW 6 substorm analysis intervals, *J. Geophys. Res.*, *90*, 1205–1216, doi:10.1029/JA090iA02p01205.

Baker, J. B., A. J. Ridley, V. O. Papitashvili, and C. R. Clauer (2003), The dependence of winter aurora on interplanetary parameters, *J. Geophys. Res.*, *108*(A4), 8009, doi:10.1029/2002JA009352.

Baumjohann, W. (1986), Merits and limitations of the use of geomagnetic indices in solar wind-magnetosphere coupling studies, in *Solar Wind-Magnetosphere Coupling*, edited by Y. Kamide and J. A. Slavin, pp. 3–15, Terra Sci., Tokyo.

Baumjohann, W., and R. A. Treumann (1997), *Basic Space Plasma Physics*, Imp. Coll. Press, London.

Baumjohann, W., R. J. Pellinen, H. J. Opgenoorth, and E. Nielsen (1981), Joint two-dimensional observations of ground magnetic and ionospheric electric fields associated with auroral zone currents: Current systems associated with local auroral break-ups, *Planet. Space Sci.*, *29*, 431–447, doi:10.1016/0032-0633(81)90087-8.

Boström, R. (1964), A model of the auroral electrojets, *J. Geophys. Res.*, *69*, 4983–4999, doi:10.1029/JZ069i023p04983.

Cai, X., C. R. Clauer, and A. J. Ridley (2006), Statistical analysis of ionospheric potential patterns for isolated substorms and sawtooth events, *Ann. Geophys.*, *24*, 1977–1991, doi:10.5194/angeo-24-1977-2006.

Carlson, C. W., and M. C. Kelley (1977), Observation and interpretation of particle and electric field measurements inside and adjacent to an active auroral arc, *J. Geophys. Res.*, *82*, 2349–2360, doi:10.1029/JA082i016p02349.

Chun, F. K., D. J. Knipp, M. G. McHarg, G. Lu, B. A. Emery, S. Vennerstrøm, and O. A. Troshichev (1999), Polar cap index as a proxy for hemispheric Joule heating, *Geophys. Res. Lett.*, *26*, 1101–1104, doi:10.1029/1999GL900196.

Clauer, C., and Y. Kamide (1985), DP 1 and DP 2 current systems for the March 22, 1979 substorms, *J. Geophys. Res.*, *90*, 1343–1354, doi:10.1029/JA090iA02p01343.

Coroniti, F. V., and C. F. Kennel (1972), Polarization of the auroral electrojet, *J. Geophys. Res.*, *77*, 2835–2850, doi:10.1029/JA077i016p02835.

Cravens, T. E. (1997), *Physics of Solar System Plasmas*, Cambridge Univ. Press, Cambridge, U. K.

Faynberg, E. B. (1975), Separation of the geomagnetic field into a normal and anomalous part, *Geomagn. Aeron., Engl. Transl.*, *15*, 117–121.

Galand, M., and A. D. Richmond (2001), Ionospheric electrical conductances produced by auroral proton precipitation, *J. Geophys. Res.*, *106*, 117–125, doi:10.1029/1999JA002001.

Germany, G. A., G. K. Parks, M. Brittnacher, J. Cumnock, D. Lummerzheim, J. F. Spann, L. Chen, P. G. Richards, and F. J. Rich (1997), Remote determination of auroral energy characteristics during substorm activity, *Geophys. Res. Lett.*, *24*, 995–998, doi:10.1029/97GL00864.

Henderson, M. G., G. D. Reeves, R. Skoug, M. F. Thomsen, M. H. Denton, S. B. Mende, T. J. Immel, P. C. Brandt, and H. J. Singer (2006), Magnetospheric and auroral activity during the 18 April 2002 sawtooth event, *J. Geophys. Res.*, *111*, A01S90, doi:10.1029/2005JA011111.

Kamide, Y., and W. Baumjohann (1985), Estimation of electric fields and currents from international magnetospheric study magnetometer data for the CDAW 6 intervals: Implications for substorm dynamics, *J. Geophys. Res.*, *90*, 1305–1317, doi:10.1029/JA090iA02p01305.

Kamide, Y., and S. Matsushita (1979), Simulation studies of ionospheric electric fields and currents in relation to field-aligned currents: 1. Quiet periods, *J. Geophys. Res.*, *84*, 4083–4098, doi:10.1029/JA084iA08p04083.

Kamide, Y., A. D. Richmond, and S. Matsushita (1981), Estimation of ionospheric electric field, ionospheric currents and field-aligned currents from ground magnetic records, *J. Geophys. Res.*, *86*, 801–813, doi:10.1029/JA086iA02p00801.

Kamide, Y., et al. (1994), Ground-based studies of ionospheric convection associated with substorm expansion, *J. Geophys. Res.*, *99*, 19,451–19,466, doi:10.1029/94JA01625.

Kan, J. R. (2007), On the formation of near-Earth X-line at substorm expansion onset, *J. Geophys. Res.*, *112*, A01207, doi:10.1029/2006JA012011.

Lu, G., et al. (1998), Global energy deposition during the January 1997 magnetic cloud event, *J. Geophys. Res.*, *103*, 11,685–11,694, doi:10.1029/98JA00897.

Lui, A.T.Y., T. Hori, S. Ohtani, Y. Zhong, X.-Y. Zhou, M. G. Henderson, T. Nagai, T. Mukai, and S. B. Mende (2004), Magnetotail behavior associated with "sawtooth injections," *J. Geophys. Res.*, *109*, A10215, doi:10.1029/2004JA010543.

Lummerzheim, D., M. Brittnacher, D. Evans, D. A. Germany, G. K. Parks, M. H. Rees, and J. F. Spann (1997), High time resolution study of the hemispheric power carried by energetic electrons into ionosphere during the May 19/20, 1996 auroral activity, *Geophys. Res. Lett.*, *24*, 987–990, doi:10.1029/96GL03828.

Matsuo, T., A. D. Richmond, and D. W. Nychka (2002), Modes of high-latitude electric field variability derived from DE-2 measurements: Empirical orthogonal function (EOF) analysis, *Geophys. Res. Lett.*, *29*(7), 1107, doi:10.1029/2001GL014077.

Mozer, F. S. (1971), Origin and effects of electric fields during isolated magnetospheric substorms, *J. Geophys. Res.*, *76*, 7595–7608, doi:10.1029/JA076i031p07595.

Newell, P. T., K. Liou, T. Sotirelis, and C.-I. Meng (2001), Auroral precipitation power during substorms: A Polar UV Imager-based superposed epoch analysis, *J. Geophys. Res.*, *106*, 28,885–28,896, doi:10.1029/2000JA000428.

Ohtani, S., et al. (2007), Cluster observations in the inner magnetosphere during the 18 April 2002 sawtooth event: Dipolarization and injection at $r = 4.6\ R_E$, *J. Geophys. Res.*, *112*, A08213, doi:10.1029/2007JA012357.

Perreault, P., and S.-I. Akasofu (1978), A study of geomagnetic storms, *Geophys. J. R. Astron. Soc.*, *54*, 547–573.

Rees, M. H., D. Lummerzheim, R. G. Roble, J. D. Winningham, J. D. Craven, and L. A. Frank (1988), Auroral energy deposition rate, characteristic electron energy, and ionospheric parameters derived from Dynamics Explorer 1 images, *J. Geophys. Res.*, *93*, 12,841–12,860, doi:10.1029/JA093iA11p12841.

Richmond, A. D., and Y. Kamide (1988), Mapping electrodynamic features of the high-latitude ionosphere from localized observations: Technique, *J. Geophys. Res.*, *93*, 5741–5759, doi:10.1029/JA093iA06p05741.

Ridley, A. J., and E. A. Kihn (2004), Polar cap index comparisons with AMIE cross polar cap potential, electric field, and polar cap area, *Geophys. Res. Lett.*, *31*, L07801, doi:10.1029/2003GL019113.

Rostoker, G., S.-I. Akasofu, W. Baumjohann, Y. Kamide, and R. L. McPherron (1988), The roles of direct input of energy from the solar wind and unloading of stored magnetotail energy in driving magnetospheric substorms, *Space Sci. Rev.*, *46*, 93–111, doi:10.1007/BF00173876.

Spiro, R. W., P. H. Reiff, and L. J. Maher Jr. (1982), Precipitating electron energy flux and auroral zone conductances: An empirical model, *J. Geophys. Res.*, *87*, 8215–8227, doi:10.1029/JA087iA10p08215.

Sun, W., W.-Y. Xu, and S.-I. Akasofu (1998), Mathematical separation of directly driven and unloading components in the ionospheric equivalent currents during substorms, *J. Geophys. Res.*, *103*, 11,695–11,700, doi:10.1029/97JA03458.

Sun, W., X.-Y. Zhou, and A. Du (2008), Quantitative separation of the directly-driven and unloading components of the ionospheric electric field, *Geophys. Res. Lett.*, *35*, L13104, doi:10.1029/2008GL033931.

Tanskanen, E., T. I. Pulkkinen, H. E. J. Koskinen, and J. A. Slavin (2002), Substorm energy budget during low and high solar activity: 1997 and 1999 compared, *J. Geophys. Res.*, *107*(A6), 1086, doi:10.1029/2001JA900153.

Turner, N., D. Baker, T. Pulkkinen, J. Roeder, J. Fennell, and V. Jordanova (2001), Energy content in the storm time ring current, *J. Geophys. Res.*, *106*, 19,149–19,156, doi:10.1029/2000JA003025.

Vasyliũnas, V. M., and P. Song (2005), Meaning of ionosphere Joule heating, *J. Geophys. Res.*, *110*, A02301, doi:10.1029/2004JA010615.

Vorobjev, V. G., and O. I. Yagodkina (2008), Empirical model of auroral precipitation power during substorms, *J. Atmos. Sol. Terr. Phys.*, *70*, 654–662, doi:10.1016/j.jastp.2007.08.046.

Weimer, D. (1996), A flexible, IMF dependent model of high-latitude electric potential having "space weather" applications, *Geophys. Res. Lett.*, *23*, 2549–2552, doi:10.1029/96GL02255.

Zhou, X.-Y., W. Sun, A.-M. Du, and A. Ridley (2008), Two major processes of the solar wind-magnetosphere-ionosphere coupling, *Adv. Geosci.*, *21*, 83–95.

S. B. Mende, Space Sciences Laboratory, University of California, 7 Gauss Way, Berkeley, CA 94720-7450, USA.

A. J. Ridley, Department of Atmospheric, Oceanic, and Space Sciences, University of Michigan, 2455 Hayward St., Ann Arbor, MI 48109, USA.

W. Sun, Geophysical Institute, University of Alaska Fairbanks, Fairbanks, AK 99775-7320, USA.

X.-Y. Zhou, Jet Propulsion Laboratory, California Institute of Technology, 4800 Oak Grove Dr., MS 169-506, Pasadena, CA 91109, USA. (xiaoyan.zhou@jpl.nasa.gov)